# Blue light is a universal tactic signal for

# *Escherichia coli*

‡#Tatyana Perlova, §‡#Martin Gruebele and ‡#Yann R. Chemla

‡Department of Physics, §Department of Chemistry, #Center for the Physics of Living Cells,

University of Illinois at Urbana-Champaign.

## Abstract

Blue light has been shown to elicit a tumbling response in *E. coli*, a non-phototrophic bacterium. The exact mechanism of this phototactic response is still unknown, and its biological significance remains unclear. Here, we quantify phototaxis in *E. coli* by analyzing single-cell trajectories in populations of free-swimming bacteria before and after light exposure. Bacterial strains expressing only one type of chemoreceptor reveal that all five *E. coli* receptors—Aer, Tar, Tsr, Tap and Trg—are capable of mediating a response to light. In particular, light exposure elicits a running response in Tap-only strain, the opposite of the tumbling response observed for all other strains. Light therefore emerges as a universal stimulus for all *E. coli* chemoreceptors. We also show that blue light exposure causes a reversible decrease in swimming velocity, a proxy for proton motive force. We hypothesize that rather than sensing light directly, chemoreceptors sense light-induced perturbations in proton motive force.

## Introduction

Phototaxis, the light-dependent movement of microorganisms, was first reported as early as the 19th century in certain species of purple bacteria [1]. Along with halobacteria and cyanobacteria, purple bacteria are phototrophic, i.e. they use light as a source of energy. Phototaxis confers an obvious advantage to phototrophic bacteria as it allows them to migrate to optimal illumination conditions [2,3]. *Escherichia coli,* on the other hand, is a surprising example of a non-phototrophic bacterium for which exposure to blue light results in changes in motile behavior [4–7].

*E. coli* motility is governed by a few simple principles that allow it to find the most favorable environment efficiently. *E. coli* is propelled by a bundle of helical, rotating flagella and swims by alternating between two types of motion—'runs', during which cells swim in one direction along an approximately straight path, and 'tumbles', during which cells randomly reorient. Runs correspond to counterclockwise (CCW) rotation of all flagellar motors, which results in a tight bundle of flagella propelling the cell forward. During tumbles, one or more flagella rotate clockwise (CW), breaking from the bundle and causing random reorientation of the cell before the next run [8]. The fraction of time spent tumbling—the 'tumble bias'—therefore depends on the fraction of time each flagellar motor rotates CW. Tumble bias changes in response to intracellular cues such as proton motive force (PMF) [9], or extracellular chemical cues [10], resulting in a behavior known as 'taxis'.

A simple signaling network controls this behavior (Fig. 1A) [10]. The intracellular signaling molecule CheY in its active, phosphorylated form (CheY-P), binds to the flagellar motors, causing a switch in rotational direction from CCW to CW. CheY is phosphorylated by the kinase CheA and dephosphorylated by the phosphatase CheZ. *E. coli* has five types of transmembrane receptors (Fig. 1A) of varying abundance—Tar, Tsr, Aer, Tap, and Trg—that sense a range of environmental signals [11,12]. These receptors form complexes with CheA, coupling its kinase activity to environmental conditions. For example, binding of chemical repellents to the receptors' ligand-binding domains results in increased CheA activity, a higher concentration of CheY-P, a higher probability of CW motor rotation, and therefore a higher

2

46     tumble bias. Conversely, binding of chemoattractants such as amino acids deactivates CheA,

47     resulting in lower tumble bias. Finally, CheA activity is also regulated by receptor methylation,

48     which is controlled by methyltransferase CheR and methylesterase CheB, the latter of which is

49     active only when phosphorylated by active CheA [10] (Fig. 1A). CheR and CheB regulation of

50     CheA activity generates a negative feedback loop that allows bacteria to adapt to new

51     conditions. The net effect is that *E. coli* run lengths increase as conditions become more

52     favorable, cells migrate towards a better environment, and eventually adapt as the tumble bias

53     returns to its basal value [13].

54     This signaling network is characterized by its (1) extreme sensitivity—an *E. coli* cell can

55     respond to concentration changes as small as ∼3 nM, corresponding to just a few molecules

56     per cell volume [14]; (2) wide dynamic range—a cell is sensitive to changes of up to 5 orders of

57     magnitude in concentration [10]; and (3) the ability to integrate diverse extracellular cues—not

58     just concentrations of various chemicals ('chemotaxis'), but temperature ('thermotaxis'), pH

59     ('pH-taxis'), and light ('phototaxis') [12,15,16]. Chemotaxis in *E. coli* has been studied

60     extensively and serves as a paradigm for the way living cells modulate their behavior in

61     response to environmental signals [13,17–20]. However, there have been only a handful of

62     studies on *E. coli* phototactic response [4–7], and the adaptive value of phototaxis remains

63     unclear.

64     Here, we study phototaxis by analyzing single-cell trajectories in populations of *E. coli*

65     bacteria free-swimming in 2D, before and after exposure to blue light. Our results show that light

66     is a universal tactic signal and elicits responses mediated by all 5 types of receptors.

67     Single-receptor mutant measurements confirm that Tar and Aer receptors mediate increased

68     tumbling in bacteria exposed to light, in agreement with prior studies [7]. The role of the other

69     three receptors in phototaxis was previously unknown. We find that Tsr and Trg also mediate

70     tumbling in response to light, whereas Tap mediates running response. Despite Tap being a low

71     abundance receptor, we also observe that several multi-receptor strains containing Tap exhibit

72     running responses to light. A reversible decrease in bacterial swimming velocity that we observe

73     upon light exposure suggests that light perturbs electron transport and/or proton motive force

74     (PMF). Based on these results, we propose a mechanism for a universal tactic response to light

3

75  in which *E. coli* receptors sense light-induced perturbations of PMF or parameters coupled to

76  PMF.

# Results

## Response to blue light requires at least one receptor, functional CheY, CheR and CheB

80  We analyzed swimming trajectories from thousands of cells stimulated by a turn-on or

81  turn-off of blue light (Fig. 1B; Fig 1 – figure supplement 1-3; Materials and Methods). Similarly to

82  Wright *et al.* [7], we observed wild-type *E. coli* tumble, then adapt in response to a turn-on, and

83  exhibit the opposite response to a turn-off (Fig. 1C). The light intensities needed to elicit a

84  detectable response were similar to those reported by Taylor and Koshland [4] and by Taylor *et*

85  *al. [5]*, but were significantly larger than those of Wright and co-workers—more than 300

86  mW/cm$^2$ compared to 7 mW/cm$^2$ [7]. We attribute the discrepancy to different growth conditions

87  in the latter study (Materials and Methods). When using the same substrates in growth and

88  motility media as Wright *et al.* (M9 supplemented with 5 mg/ml glycerol and motility buffer with 5

89  mM lactate) we reproduced similar responses at a lower light intensity (Fig. 1 – figure

90  supplement 4. Under our conditions (M9 supplemented with 4 mg/ml succinate and motility

91  buffer with 4 mg/ml succinate), the response amplitude increased with light intensity and

92  saturates at ~400 mW/cm$^2$ (Fig. 1C).

93  We confirmed that this response is mediated by the chemotactic network by performing

94  control experiments with mutants missing different components of the network (Fig. 1 – figure

95  supplement 5). We observed no response to light in either a receptorless strain (UU1250, Table

96  1) or a strain lacking functional CheY (CR20, Table 1). Therefore, similar to other types of tactic

97  stimuli, blue light modulates the activity of receptor signaling complexes, and this signal is

98  communicated to the flagellar motors through the signaling molecule CheY-P. Blue light does not

99  appear to affect switching of flagellar motor rotation directly.

100  We also confirmed that the observed adaptation to blue light is mediated by chemotactic

101  network proteins CheR and CheB. A strain lacking the receptor demethylase CheB (ΔB, Table

4

102    1) had a very high tumble bias which did not increase measurably upon light exposure (Fig. 1 –

103    figure supplement 5). The lack of response indicates that fully methylated receptors cannot be

104    further activated by light. A strain lacking the receptor methyltransferase CheR (ΔR, Table 1)

105    exhibited an initial sharp increase in tumble bias, similarly to the wild-type strain, but the tumble

106    bias then failed to return to a lower value (Fig. 1 – figure supplement 5). The lack of adaptation

107    is expected: in the absence of CheR, receptor methylation level is low and adaptation through

108    de-methylation is therefore impossible. In summary, the lack of response in the ΔCheB strain

109    indicates that a tumbling response to light is caused by receptor activation in the wild-type

110    strain. The post-response kinetics in the ΔCheR strain indicate that adaptation in the wild-type

111    strain is mediated by CheR through the negative feedback loop of the chemotaxis network.

112    (Note that rather than simply leveling off, the tumble bias of ΔCheR continues to increase slowly,

113    which we speculate is due to a slow, secondary effect.)

## All five *E. coli* chemoreceptors mediate blue light-induced changes in tumble bias

116    **Turn-on responses.** The results above demonstrate that the blue light response in

117    wild-type *E. coli* requires functioning receptor complexes. To determine the independent

118    contribution of individual receptor types, we measured the responses of mutants expressing

119    only a single receptor type (Materials and Methods). Abundances (i.e. copy numbers) of

120    different receptor types can span two orders of magnitude in wild-type strains [21]. Therefore,

121    low-copy-number receptors Aer, Tap, and Trg were expressed from a plasmid, with the

122    concentration of inducer adjusted to ensure that a tumble bias in the mutant strain in the

123    absence of stimulus was similar to that of the wild-type strain. Confirming the results of Wright *et*

124    *al.* [7]*,* we observed tumbling responses in Tar- and Aer-only strains (Fig. 2A). We also detected

125    responses in Tsr-, Trg-, and Tap-only strains. The Tsr-only strain exhibited a weak but consistent

126    tumbling response, and the Trg-only strain showed a tumbling response with delayed onset (Fig.

127    2A).

128    The Tap-only strain showed a unique response pattern compared to the other receptors.

129    Tap, like Trg, can be methylated, but lacks the NWETF motif that recruits the methyltransferase

130 CheR [22]. Therefore, we expected the Tap to have a low methylation level, and hence low

131 activity in the the absence of other receptors. Indeed, we observed that the Tap-only strain had

132 a significantly lower tumble bias than the wild-type strain and did not respond to blue light

133 exposure. The lack of response suggests that unlike Trg, Tap receptor is not activated by light

134 exposure. In order to explore the possibility that Tap can be deactivated by light exposure and

135 therefore mediate a running response, we performed light response measurements of the

136 Tap-only mutant in the presence of phenol. Phenol is a repellent for Tap and therefore activates

137 Tap receptors, increasing its tumble bias [23]. Indeed, the Tap-only strain had a higher tumble

138 bias in the presence of phenol which increased with phenol concentration (Fig. 2 – figure

139 supplement 1). Starting with the higher tumble bias in phenol in the dark, we observed running

140 responses to light in 2.5 mM (Fig. 2A and Fig 2 – figure supplement 1) and 5 mM phenol (Fig 2

141 – figure supplement 2). Phenol does not absorb in the blue region of the spectrum [24], which

142 rules out the possibility that Tap responds to excited-state phenol rather than to light itself.

143 Further controls with the Tar-only strain in the presence of 2.5 mM phenol (Fig 2 – figure

144 supplement 1) exhibited qualitatively the same response to light turn-on and turn-off as in the

145 absence of phenol, although the time scales of the response and adaptation were affected.

146 These results taken together indicate that unlike the Tar, Tsr, Aer, and Trg receptors, the Tap

147 receptor is deactivated by light exposure and mediates a running response in *E. coli*.

148    The observed single-receptor responses exhibited adaptation behavior consistent with

149 what is known about the mechanisms of adaptation for different receptors (Fig. 2A). Both Tar-

150 and Tsr-only strains adapted to a steady-state tumble bias <10 s after the light turn-on, which is

151 consistent with methylation-dependent adaptation (Fig. 2B). In contrast, Tap- and Trg-only

152 strains did not adapt appreciably to light turn-on, consistent with the fact that they cannot recruit

153 CheR [22]. We did observe partial, slow adaptation kinetics in both mutants, which may be due

154 to the recently reported mechanism of motor remodeling [25] or, alternatively, may reflect

155 internal dynamics of the processes perturbed by light. The Aer receptor adapts through an

156 unknown methylation-independent pathway that also tends to be slower [26] and consequently,

157 we do not observe significant adaptation for the Aer-only strain within the duration of our

158 measurement.

6

159     **Turn-off responses.** For most of the single-receptor strains, light response to light

160     turn-off was symmetrical (Fig. 2A). For example, In Tsr-only and Tar-only strains the running

161     responses to turn-off had adaptation kinetics similar to turn-on, further confirming that

162     adaptation is mediated by the negative feedback loop of the chemotaxis network (Fig. 2A). In

163     Trg and Tap-only strains, responses to light turn-off were also opposite in sign to those to

164     turn-on, but with little to no adaptation (Fig. 2A). In contrast, Aer-only strain exhibited markedly

165     slower response kinetics when high intensity light was turned off as compared to light turn on.

166     This result suggests that the effect of light goes beyond receptor activation, and that Aer may be

167     sensing a secondary effect from which it takes some time to recover, rather than light itself (Fig.

168     2A). However, at low light intensity, Aer responses to light turn-off and turn-on became

169     symmetric (Fig. 2 – figure supplement 2). This intensity dependence suggests that Aer has a

170     sensing mechanism qualitatively different at low and high light intensities.

171     **Response time analysis.** We also analyzed the response times—defined as the time

172     from the application of the stimulus to the response peak—of the various strains. We switched

173     light on and off in less than one movie frame (0.08 s), and conformational changes of receptors

174     in response to stimuli are known to happen on a sub-second time scale [27]. Slower response

175     times may indicate that receptors are responding to the light-induced perturbations of cellular

176     processes on longer timescales, rather than responding directly to light. Response to light

177     exposure was immediate within the time resolution of the experiment for Tar, Tsr and Aer-only

178     strains at high light intensity, while both Tap and Trg-only strains demonstrated gradual

179     responses (Fig. 2A). In the latter cases, response kinetics likely reflect the dynamics of

180     secondary processes caused by light. Our measurements cannot distinguish whether the

181     observed gradual response kinetics result from a uniformly slower response across the cell

182     population or from immediate single-cell level responses with varying time delays [28].

183     Single-cell taxis assays that provide long (~100 s) tumble bias traces for individual bacteria may

184     allow distinguishing between these two explanations [28].

185     Figure 2B summarizes the dependence of the response amplitudes, response times, and

186     adaptation times on light intensity for representative strains. There are several trends worth

187     noting. First, the amplitude of the response to light exposure increased with intensity and

7

188 saturated at around 400 mW/cm$^2$, similarly to wild-type (Fig. 2B, left panels). This is in contrast

189 with the results of Wright *et al.* who reported saturation above ∼10 mW/cm$^2$ [7]. However, as

190 shown above, growth conditions appear to affect the sensitivity of the response (Fig. 1 – figure

191 supplement 4). Although the peak tumble bias at saturating light intensity for single-receptor

192 mutants is higher than for the wild-type strain, it is still lower than that for continuously tumbling

193 bacteria (Fig. 2A). Response times to light turn-on in Aer and Trg-only strains decreased with

194 light intensity (Fig. 2B, middle panels). No dependence of response and adaptation times on

195 light intensity was observed for Tar-only strain (Fig. 2B, middle and right panels).

## Contribution of individual receptors to the light response in multiple receptor strains is non-additive

198 Our results indicate that light is a universal tactic stimulus that affects all five *E. coli*

199 chemotactic receptors. When all receptors respond to the same stimulus, it is far from obvious

200 how the signals from different receptors will be integrated to produce a response in wild-type

201 strain. Chemotaxis signaling units, formed by trimers of receptor homodimers and CheA dimers,

202 are organized into a hexagonal lattice that serves as a structural platform for interactions

203 between receptors [29–31]. Signals from low abundance receptors are thus amplified by

204 interactions with high abundance receptors and could still contribute to the chemotactic

205 response [32]. Therefore, the contribution of individual receptor types to the overall response

206 could be non-additive.

207 As shown in Fig. 1, in a wild-type strain the integrated result of the individual receptor

208 contributions is a tumbling response. The tumbling response is followed by an undershoot,

209 which has been proposed to result from receptor interactions [33]. The response amplitude of

210 the wild-type strain, in which 4 out of 5 receptors (all but Tap) mediate a tumbling response to

211 light, is comparable to that of the Tar-only strain. This suggests that, despite its low abundance,

212 the 'running' receptor Tap may contribute to the response of the wild-type strain and lower the

213 amplitude of the tumbling response.

214 Since Tap is the only receptor type to mediate a running response to light exposure, we

215 asked whether it can switch the sign of the response in multi-receptor mutants, strains

8

216  expressing a subset of 5 chemoreceptors (Table 1). Indeed, we observed a running response in

217  several mutants containing the Tap receptor (Fig. 3). For example, a combination of

218  high-abundance Tar and low-abundance Aer receptors, which both mediate tumbling responses,

219  and low-abundance Tap receptor produced a running response as illustrated by the ΔTsrΔTrg

220  strain (Fig. 3A). Similar to the Tap-only strain, the response in this mutant was not immediate, as

221  it took ~5 s to reach the minimum in tumble bias. Turning the light off also caused a tumbling

222  response, although with much lower amplitude. We also observed a running response to a light

223  turn-on in a ΔAer strain, with a similarly slow response time (Fig. 3A). In these strains, we

224  expect receptor abundance to be similar to that in the wild-type strain—where the abundance of

225  Tap is much lower than that of Tar or Tsr (Fig. 3C). Therefore, the running response must be a

226  result of amplification of Tap-mediated signaling by other receptors.

227        We found that the presence of Tap was a necessary, but not sufficient condition to

228  observe a running response. For example, adding Tsr receptor to ΔTsrΔTrg mutant resulted in a

229  switch in response from running back to tumbling (Fig. 3A, B). This result is especially surprising

230  given that Tsr only mediates a weak tumbling response on its own (Fig. 2), the addition of Tsr

231  can overwhelm the running response caused by addition of Tap, restoring a more wild-type-like

232  tumbling response. This further underlines the importance of interactions between receptors in

233  determining the overall response.


234  **Blue light exposure causes a reversible decrease in swimming velocity**

235        Despite primarily sensing different environmental signals, the 5 chemoreceptors in *E. coli*

236  universally respond to the same blue light stimulus, one of them in the opposite direction from

237  the other four. According to current understanding, Aer is the only receptor that binds a blue

238  light-absorbing chromophore (flavin adenine dinucleotide, FAD) as a cofactor, and therefore

239  could be directly photosensitive [34]. Thus, the mechanism of photosensitivity is unclear for the

240  remaining four receptors. It has been speculated that *E. coli* monitors some intracellular

241  parameter perturbed by absorption of blue photons. Wright and co-authors suggested, for

242  example, that the Tar receptor may be sensing perturbations in electron transport induced by

9

243 blue light, which would affect Proton Motive Force (PMF) [7]. We explored whether or not the

244 PMF hypothesis is a plausible explanation for the light sensitivity of chemoreceptors.

245 PMF is generated during respiration by electron and proton translocation across the

246 membrane [35]. It is used to generate ATP and to energize other processes in the cell such as

247 ion transport and flagellar rotation [35]. It was previously shown that the flagellar rotation rate is

248 linearly proportional to PMF under both high and low viscous load, the latter corresponding to

249 the load on flagella in free-swimming bacteria [36,37]. Therefore, all else being equal, the

250 bacterial swimming velocity can serve as a proxy measure of PMF. If the light does affect PMF,

251 we can expect to see corresponding trends in swimming velocity.

252 Velocity traces for receptorless strain UU1250 at different light intensities are shown in

253 Figure 4A. Light exposure caused a gradual decrease in its swimming velocity. Since the

254 receptorless strain does not exhibit a change in tumble bias in response to light (Fig. 1 – figure

255 supplement 4), trends in swimming velocity cannot be attributed to an imperfect run-tumble

256 assignment (see Materials and Methods). A similar decrease in velocity was also observed for

257 all other strains assayed, including the wild-type (Fig. 4B). The magnitude of the decrease in

258 normalized swimming velocity after 30 s of light exposure, $\Delta v_{on}$, depends on the light intensity

259 and varies from 0 at ≤44 mW/cm$^2$ to about 8% at 550 mW/cm$^2$ on average (Fig. 4B). Moreover,

260 the velocity decrease appears reversible. About 50% of the velocity decrease is recovered

261 within 30 s after the light is turned off at all intensity levels. It is likely that a full recovery can be

262 achieved with sufficient waiting time, but our assay preclude measurements beyond ~30 s.

263 Under our experimental conditions we cannot distinguish between a velocity recovery in

264 previously exposed bacteria and a velocity increase due to unexposed bacteria swimming in the

265 field of view after 30 s (Materials and Methods). Nevertheless, our results strongly suggest a

266 reversible decrease in velocity, which is consistent with reversible perturbation of PMF by blue

267 light exposure as opposed to irreversible motor photodamage.

268 ## Discussion

269 A tumbling response to blue light in *E. coli* was first demonstrated in 1975 [4]. Later,

10

270    Wright *et al.* [7] identified two types of receptors essential for the tumbling response to blue light:

271    Tar and Aer. Our work shows that the response to light in *E. coli* is mediated by all of the

272    receptor types, including Tsr, Trg and Tap. Downstream from the receptors the effect of light on

273    the chemotaxis network is consistent with that of other tactic stimuli. Light thus emerges as a

274    universal tactic stimulus that affects all five *E. coli* chemoreceptors. While 4 out of 5 receptors

275    mediate tumbling, or a repellent response to light, Tap receptor mediates running, or an

276    attractant response. We find that, despite being a low-abundance receptor, Tap is capable of

277    determining the direction of light response in multi-receptor mutants, likely aided by amplification

278    of Tap-mediated signaling by other receptors.

279    Our results on the effect of light on swimming velocity are consistent with the hypothesis

280    that blue light perturbs electron transport or affects PMF, as well as with the previous

281    observation that phototaxis in *E. coli* requires a functioning electron transport chain [5]. The

282    mechanism of PMF perturbation is not clear and our experiments do not provide information that

283    would help to elucidate it. However, we speculate that light causes photoreduction of electron

284    carriers such as FAD in the cytoplasmic pool, thereby disrupting electron transport. FAD is a

285    good candidate carrier as it absorbs in the blue spectral region and is known to undergo

286    photoconversion between its different redox and protonation states as a co-factor of LOV and

287    BLUF flavoprotein light sensors [38–40].

288    The different response kinetics that we observe for single-receptor mutants may reflect

289    different blue light sensing mechanisms of individual receptors (Figure 2 and Figure 2 - Figure

290    supplement 2). Response times appear to fall into two categories—fast (e.g. Tar), in which the

291    response is essentially immediate within the time resolution of our measurements and likely

292    reflect a direct light absorption process, and slow (e.g. Trg), in which light-induced changes are

293    presumably more indirect and take longer to have an effect. In the Aer-only strain, the response

294    is essentially immediate at higher intensities, which is consistent with direct sensing of light by

295    Aer through the photoreduction of its co-factor FAD [41]. On the other hand, as a receptor for

296    'energy-taxis,' Aer can also sense perturbations in electron transport, proposed to occur through

297    change in redox state of respiratory enzymes [42]. We speculate that this sensing mechanism is

298    reflected in the slower response times observed at lower light intensities (Figure 2 - figure

11

299   supplement 2). In contrast, Tsr has been shown to respond directly to changes in PMF, and may

300   display fast response kinetics due to the low threshold needed to elicit a response [42]. How the

301   remaining receptors sense light remains unclear. Based on the response kinetics we suspect

302   that Tar responds to light or parameters that change immediately with light intensity, while Tap

303   and Trg sense more indirect light-induced effects (Figure 2).

304   To place our results in perspective, we compare the intensity values that we have used

305   with those that bacteria may actually encounter in nature. *E. coli* bacteria live a biphasic lifecycle

306   with their primary habitat in the mammalian gut. Between being excreted from one host and

307   finding the next one, *E. coli* bacteria inhabit nutrient-sparse water or soil environments [43].

308   During the environmental phase of its lifestyle, *E. coli* can be exposed to the light from the sun.

309   The intensity of the solar illumination at the surface of Earth is ~140 mW/cm$^2$ across the visible

310   spectrum, with roughly 60 mW/cm$^2$ falling within the 60 nm band of the blue light response

311   spectrum as measured by Wright *et al.* [7]. This value is comparable to the lowest intensity at

312   which we observed significant responses for some of the strains in this study, 74 mW/cm$^2$ (Fig.

313   2), although not for the wild-type strain (Fig. 1). However, under different growth conditions the

314   wild-type strain exhibits a clear response at these low light intensities (Fig. 1 – figure

315   supplement 4) consistent with observations by Wright and co-workers [7]. We speculate that the

316   blue light response depends on growth conditions because they affect the relative abundances

317   of different receptors types [21,44], which strongly affect its amplitude and sign according to our

318   data for multi-receptor mutants (Fig. 3). Therefore, responses may be more significant for some

319   free-living *E. coli* strains. While it remains to be seen what the biological significance of the blue

320   light response is, our results indicate that migration of *E. coli* bacteria due to exposure to

321   sunlight is plausible.

322   We also propose that blue light may be a useful tool in investigations of chemotactic

323   behavior. Because light is a universal stimulus for all *E. coli* receptors, it may provide a way to

324   quantify interactions between different types of receptors, through simulating the behavioral

325   output of the chemotaxis network in response to light and fitting to the experimental data. In

326   addition, light, unlike chemicals, is much easier to control both in time and in space. Therefore,

327   using light as a stimulus may allow studying taxis behavior of bacteria in a heterogeneous

12

328 environment with multiple light gradients, thereby bridging the gap between the types of
329 gradients bacteria likely encounter in nature and those that can be generated experimentally.

## Materials and Methods

### Microbiology

#### Cell growth and media

333      Bacteria were grown for 20-24 hours overnight from a single colony in 1 ml of M9
334 minimal medium, supplemented with 4 mg/ml succinate unless otherwise noted (1x M9 salts:
335 12.8 g/l $Na_2HPO_4 \cdot 7H_2O$, 3g/l $KH_2PO_4$, 0.5 g/l NaCl, 1 g of $NH_4Cl$; 2 µM $MgSO_4$; 0.1 mM $CaCl_2$;
336 0.5 mM of each Meth, Leu, Thr and His; 100 µg/ml thiamine; 4 mg/ml succinate) shaking at 265
337 RPM at 30°C with appropriate antibiotics if necessary (34 µg/l of Chloramphenicol or 100 µg/l of
338 Ampicillin). The overnight culture was diluted 50-fold in 1 ml of the same medium and grown,
339 shaking at 265 RPM at 30°C for 8-12 hr (to OD600 ~0.25-0.3) with appropriate inducers if
340 necessary. The following concentrations of inducers were used for strains with plasmids: 50 µM
341 IPTG for UU1250 + pSB20, 0.7 µM NaSal for UU1250 + pTP1 and 0.8 µM NaSal for UU1250 +
342 pPA705.

343      The over-day culture was harvested by centrifugation (1300 g, 10 min) and gently
344 resuspended in the appropriate volume of "motility buffer" [28] (70 mM NaCl, 100 mM Tris-Cl pH
345 7.5, 4 mg/ml succinate, 100 µM methionine) to reach a final OD of 0.15. Bacteria were placed
346 back in the shaker to oxygenate the media. Methionine was added to a final concentration of
347 100 µM prior to sample chamber assembly. Phenol was added to a final concentration of 2.5
348 mM or 5 mM where noted.

#### Strains

350 Bacterial strains and plasmids used in this study are listed in Tables 1 and 2. Plasmid pTP1 was
351 constructed from plasmid pKG117 by subcloning the wild-type *tap* gene between NdeI-BamHI
352 restriction sites (Table 2). Synthesis and subcloning were performed by Genscript.

**Two-dimensional swimming assay**

Slides (3" x 1", # 3010, Thermo-Fisher) and coverslips (22 x 22 mm, #1, VWR) were sonicated in acetone for ~15 min, rinsed, then sonicated in KOH for 15 min, and rinsed and dried by centrifugation (1000 rpm, 3 min). Cleaning was done on the day of each experiment as we found that storing cleaned slides in distilled water even for one day resulted in the accumulation of defects on the glass surface. Prior to each experiment, slides and coverslips were passivated with bovine serum albumin (BSA, B9000S, New England BioLabs) to prevent sticking of bacteria. Slides and coverslip were incubated with 2 mg/ml BSA for ~20 min, then rinsed with a copious amount of water and dried with nitrogen. To assemble the chamber, a drop of motility buffer (5 µl) containing *E. coli* cells was placed on a slide and gently covered with a coverslip. Care was taken to prevent the formation of air bubbles. To prevent buffer evaporation, open sides were sealed with fast curing epoxy (Devcon, 5 minute epoxy). The distance between the slide and coverslip was determined by the thickness of the liquid layer of bacterial medium and was ~10 µm, which roughly corresponds to our 20x objective's depth of field.

# Microscopy

We used an inverted optical microscope (Zeiss, Axio Observer A1) with a 20x objective (Zeiss, A-Plan 20x/0.45 M27) in phase contrast mode to image swimming bacteria. For observation, bacteria were illuminated from the top by a halogen lamp (HAL 12V/100W). Light from the lamp was heat filtered and passed through a 500-nm long-pass filter (Chroma, ET500lp) to exclude the possibility of excitation of bacteria by the observation light (Fig. 1b).

Excitation light from a blue LED was introduced through the back port of the microscope. A blue LED (Thorlabs, M455L3) with a collimation assembly (retaining ring, lens tube, and aspheric condenser lens (Thorlabs, ACL2520-A)) was mounted using a Zeiss Axioskop Microscope Lamphouse Port Adapter (Thorlabs, SM1A23). Excitation light passed through a 440 ± 5-nm bandpass filter (Chroma, CT440/10bp) and was directed toward the field of view by a 500-nm dichroic mirror (Chroma, 500dcxr). To achieve even illumination of the field of view, we followed the standard procedure for Koehler illumination. The microscope field stop was opened to match the field of view (≈1.2 mm in diameter for the 20x objective).

14

381        The output light intensity of the LED was determined by the current from the LED driver

382     (Thorlabs, LEDD1B) controlled by a DAQ card (National Instruments, NI PCI-6221) and defined

383     using a LabView interface. Neutral density filters of ND 1 and ND 0.5 were installed in the filter

384     slider (Thorlabs, NE05B ND, and NE10B ND) to gain finer control over the resulting light

385     intensity. Light intensity at the sample plane at different supply voltages was measured with a

386     power meter (Newport, power meter 1916C equipped with photodiode sensor 918D-SL-OD3)

387     placed on the microscope stage such that the illumination fitted the area of the sensor. To

388     calculate light power density, the total power was divided by the illumination area. The

389     unevenness of the illumination was estimated from the distribution of pixel brightness values in

390     an image taken by the camera below its saturation and was found to be ~10% of the mean. We

391     used this value as an estimate for the error in light power density.

392        Movies of swimming bacteria were captured using a CCD camera (PointGrey,

393     Grasshopper 3) mounted at the microscope side port. Camera calibration with USAF target

394     1951 (Thorlabs, R3L3S1P) gave us an estimate of the pixel size of ~0.26 µm. The size of the

395     area captured by the camera in the sample plane was 532 x 532 µm. Movies were recorded at a

396     frame rate of 12 frames per second.

## Data analysis

### Trajectory preparation and filtering

399        Analysis of bacterial trajectories was performed using an automated workflow

400     implemented in Python. First, we detected bacteria in each frame of a recorded movie using the

401     OpenCV computer vision library [45]. Then, coordinates were linked into trajectories using the

402     trackPy package (Fig. 1B) [46]. At this point, we removed all trajectories shorter than 1 s, or 12

403     frames, from further consideration. Then we calculated instantaneous linear velocities and

404     accelerations and angular velocities and accelerations using 1-frame windows following the

405     procedure described by Dufour *et al.* [47].

406        Next, we used the following approach to filter out spurious trajectories that belonged to

407     bacteria tethered to the surface, drifting, or swimming too slowly. For every trajectory, we

408     calculated the average angular velocity and the 95th percentile of the linear velocity. The

409 two-dimensional distribution of all trajectories in these coordinates contains two clusters: one

410 cluster corresponding to normally swimming bacteria, the less populated cluster containing

411 trajectories of very slow or surface-tethered bacteria (Fig. 1 – figure supplement 3). For each

412 bacterial strain, we found the two coordinates of the maximum of the 'swimming' cluster—the

413 most probable values of angular velocity and 95th percentile of velocity—and kept only the

414 trajectories that lied within the a certain radius $R$ from the maximum. With the exception of the

415 few strains that exhibit a very strong response to light, we defined $R$ as $R = 4 <MAD>$, where $<$

416 $MAD >$ is the median absolute deviation (MAD) from the maximum of the distribution, averaged

417 across all strains with a functional chemotaxis network. Filtering was performed separately for

418 different strains to avoid bias due to variation in the swimming behavior. We found that filtering

419 does not affect trajectories of the bacteria that are exposed to light disproportionately: the

420 fraction of trajectories within $4 < MAD >$ for bacteria before, during, and after light exposure is

421 roughly the same.

422 The area accessible to bacteria in a slide-coverslip chamber is larger than the

423 illuminated area. Therefore, unexposed bacteria swimming from outside of the area illuminated

424 by blue light could subsequently swim into the field of view and affect the observed kinetics.

425 However, the illuminated area is still larger than the observation area captured by the camera,

426 and these bacteria have to swim $0.2 – 0.3$ mm to reach the field of view. To estimate on what

427 time scale these bacteria could contribute to the observed kinetics, we calculated the Mean

428 Square Displacement (MSD) for trajectories of the wild-type *E. coli* (strain RP437) as a function

429 of time. From a power law fit of the MSD, we estimate that it will take unexposed bacteria at

430 least 30 s to reach the field of view, although the time will vary for different strains depending on

431 the swimming velocity and tumbling frequency. Based on this estimate we only consider the

432 portions of tumble bias and velocity time traces within 30 s after the light has been turned off or

433 on.

434 **Run-tumble assignment**

435 To assign run and tumble states we used a Hidden Markov Model with

436 Gaussian-distributed emissions similar to the one described by Dufour *et al.* [47]. In this type of

16

437 model, the state of the system (e.g. 'run' or 'tumble') is not directly observed ('hidden'), but its
438 outputs ('emissions') such as velocity, acceleration, and angular acceleration can be observed.
439 The hidden states and known outputs are related by an emission probability, while the transition
440 between states is given by a transition matrix.

441 We implemented the Hidden Markov model using the Python package *hmmlearn* to infer
442 the sequence of 'hidden' swimming states from time traces of the observable parameters [48].
443 Parameters of the model—the transition probability matrix and the emission probabilities of the
444 observables—are estimated from a reference dataset consisting of >20,000 pre-stimulus
445 trajectories of wild-type bacteria. Training is done iteratively. At each iteration, velocities and
446 accelerations are normalized by the average swimming velocity (the 95th percentile of the
447 velocity is used over the first iteration), model parameters are estimated from a resulting
448 sequence of observables and an optimal sequence of states is inferred. The process is repeated
449 until the change in normalized velocity between two consecutive iterations is below 2%. To
450 account for the variation in swimming velocity within one trajectory, we used a model with three
451 states—'fast run', 'slow run', and 'tumble'. The running velocity was calculated from states
452 corresponding to a fast run. While we performed run-tumble assignment for all the collected
453 trajectories, only those longer than 100 frames were used for all the plots in the paper, as
454 shorter trajectories do not contain enough points for accurate run-tumble assignment as shown
455 by Dufour *et al.* [47].

456 We validated our assignment by comparing tumble bias time traces obtained with the
457 above analysis to those obtained with alternative run-tumble assignment criteria introduced by
458 Alon *et al.* [49]. Under these alternate criteria, bacteria were considered to be tumbling if the
459 velocity was below the 90th percentile of velocities divided by two and if the angular velocity was
460 above 6 rad/s. We compared tumble bias traces obtained with each assignment method.
461 Although the absolute value of tumble bias was offset depending on the specific method used to
462 assign runs and tumbles, the trends—response and adaptation to light exposure—did not
463 depend on the analysis method. Finally, following Wright *et al.* we used angular velocity or RCD
464 [7] (rate of change in direction), which is proportional to tumble bias over a range of values [50],
465 as a population measure of the *E. coli* chemotactic response. We found similar trends in the

17

466 RCD traces as well. Therefore, we conclude that our results are robust to the method of

467 analysis. The Python library that we developed for detection and analysis of trajectories is

468 available on the GitHub repository: https://github.com/tatyana-perlova/py-taxis.

469      For each movie, the average tumble bias across all trajectories was calculated in each

470 movie frame. Tumble bias traces from movies taken under the same conditions were averaged,

471 yielding a smooth tumble bias trace as a function of time for each strain or condition. We used

472 standard error between the tumble biases of individual bacterial trajectories as a measure of

473 uncertainty of average tumble bias (Fig. 1C, shaded area). The amplitude $A$ was defined as the

474 maximum change in tumble bias upon light exposure compared to the pre-stimulus value and

475 was calculated over a 0.5-s window to minimize the contribution of noise (Fig. 2B). For

476 extracting response and adaptation times, tumble bias response traces during light exposure

477 were fitted to the equation:

478 $$TB(t) = A_0 + A_1 exp\left(-\frac{t}{\tau_1}\right) + A_2 exp\left(-\frac{t}{\tau_2}\right) + A_3 log\left(\frac{t+0.01}{\tau_3}\right)$$

479 The logarithmic term was added to account for the slow adaptation kinetics in some of the

480 receptor mutants. The response time $t_{resp}$ was defined as the time it takes for the resulting fitted

481 function to reach 90±1% of the amplitude (Fig. 2B) or:

482 $$|F(t_{resp}) - TB(t<0) - 0.9A|/A \leq 0.01$$

483 Similarly, the adaptation time $t_{adap}$ was defined as the time it takes for the difference between the

484 pre-stimulus value of tumble bias and the fitting function to reach 50±1% of the amplitude (Fig.

485 2B). The error in determining response and adaptation time was calculated as the standard

486 error of the tumble bias at $t_{resp}$ or $t_{adap}$ (width of the shaded area around the tumble bias trace,

487 Figure 2) divided by the slope of the linear fit to the trace at that point. For plotting, tumble bias

488 time traces were averaged using a 10-frame moving window.

489 **Running velocity analysis**

490      The running velocity was defined as the velocity during frames assigned to runs. For the

491 non-tumbling receptorless strain UU1250 we used velocity during every frame. Time traces of

492 the normalized run velocity (Fig. 4A) were calculated as follows: each individual velocity trace

493 was divided by the pre-stimulus velocity calculated in a 20-s window prior to light exposure.

494    Traces for were then shifted to align 'light on' or 'light off' frames and averaged using a 10-frame

495    non-overlapping rolling window. As the tumble assignment procedure is not perfect, not all

496    tumbles are detected, which is reflected in a sudden decrease in swimming velocity right after

497    light exposure for strains with a tumbling response to light (data not shown). To measure the

498    effect of light on the running velocity while minimizing the effect of false negatives we use the

499    following procedure: for each individual movie velocities are calculated in a 4-s windows after 30

500    s of light exposure and then 10, 20 and 30 s after the light is turned off (Figure 4B). Therefore

501    we do not take into account velocity right after the light is turned on. In Aer-only and Trg-only

502    strains, tumble bias does not return to pre-stimulus values even after 30 s of exposure.

503    Therefore these strains were excluded from this analysis. Observation was limited to 30 s to

504    avoid contribution of unexposed bacteria swimming into the field of view. Velocities calculated in

505    this way for each trace were then normalized to the pre-stimulus velocity calculated in a 20-s

506    window and averaged across all the traces for a particular strain. Decrease and recovery of

507    normalized run velocity were calculated as illustrated in Fig. 4B by averaging data points for

508    different strains. The velocity decrease, $\Delta v_{on}$, was an average decrease of normalized run

509    velocity after 30 s of light exposure. The velocity recovery characterizes the fraction of $\Delta v_{on}$

510    recovered 30 s after light turn-off and was calculated as $(\Delta v_{on} - \Delta v_{off})/\Delta v_{on}$ (Fig. 4B).

19

511    Table 1. Strains used in this work

| Strain | Genotype | Comments | Source |
|---|---|---|---|
| RP437 | | Wild-type chemotaxis strain | [51] |
| ΔR | ΔcheR | | Christopher Rao |
| ΔB | ΔcheB | | Christopher Rao |
| CR20 | CheY::FRT | Runner | Christopher Rao [52] |
| UU1250 | Δ(tar-tap), Δtsr, Δaer, Δtrg | Receptorless strain | John S. Parkinson [26] |
| UU1615 | Δaer Δtar Δtap Δtrg | Tsr-only strain | John S. Parkinson [53] |
| UU1624 | Δaer Δtsr Δtap Δtrg | Tar-only strain | John S. Parkinson [53] |
| UU1250 + pSB20 | Δ(tar-tap) Δtsr Δaer, Δtrg | Aer-only strain, contains pSB20 plasmid | John S. Parkinson [7] |
| UU1250 + pPA705 | Δ(tar-tap) Δtsr Δaer, Δtrg | Trg-only strain, contains pPA705 plasmid | This work |
| TP6 | Δ(tar-tap) Δtsr Δaer Δtrg | Tap-only strain, contains pTP1 plasmid | This work |
| RP8604 | Δtsr Δtrg | Tar-Aer-Tap strain | John S. Parkinson |
| RP1131 | trg::Tn10 | ΔTrg strain | John S. Parkinson |
| UU1117 | Δaer | ΔAer strain | John S. Parkinson [54] |

20

574 Table 2. Plasmids used in this work

| Plasmid | Genotype | Comments | Source |
|---------|----------|----------|--------|
| pSB20 | Aer, Amp$^R$ | IPTG-inducible wild-type Aer | [7] |
| pPA705 | Trg, Cm$^R$ | NaSal-inducible wild-type Trg | [29] |
| pKG117 | Aer, Cm$^R$ | NaSal-inducible wild-type Aer | [7] |
| pTP1 | Tap, Cm$^R$ | NaSal-inducible wild-type Tap | This work |

21

599 **Figure 1. Phototaxis in _E. coli._** (A) Schematic of the chemotaxis network. Five types of
600 chemoreceptors (Tar, Tsr, Aer, Trg, and Tap) sensitive to different extra- and intracellular cues
601 modulate the activity of the kinase CheA, which phosphorylates the signaling molecule CheY.
602 Phosphorylated CheY binds to flagellar motors causing them to switch to clockwise (CW)
603 rotation. Chemotactic adaptation is mediated by methyltransferase CheR and methylesterase
604 CheB. Methylation of receptor sites (black circles) by CheR increases kinase activity. CheB,
605 when phosphorylated by active CheA, de-methylates receptors (white circles) and decreases
606 kinase activity. (B) Experimental and data analysis framework for studying phototaxis in _E. coli_.
607 An inverted light microscope with 20x objective (O) with wide-range HAL lamp (yellow light path)
608 images swimming cells, and a blue LED (blue light path) stimulates cells. Movies of swimming
609 bacteria are captured by a CCD camera. Bacteria are detected in each movie frame and their
610 coordinates are linked into trajectories, which are filtered and analyzed to assign runs (blue
611 lines) and tumbles (red circles). (C) Response of the wild-type strain RP437 (schematic
612 indicates that all receptor types are present) to a turn-on and turn-off in blue light of intensity 551
613 $\pm$ 55 mW/cm$^2$. Light exposure is indicated by the shaded area as well as by the light intensity
614 profiles above the plots. Each point on the time trace is the average of the tumble biases of
615 ~6000-7000 trajectories. The shading around the time trace represents the standard error of the
616 mean tumble bias. (D) Amplitude of the response to turn-on (filled circles) and turn-off (empty
617 circles) as a function of light intensity.

618 **Figure 1 – figure supplement 1. Experimental setup.** (A) Schematic of the setup with the light
619 paths indicated by yellow (wide-range visible light from HAL lamp) and blue (blue LED) lines.
620 Components are labeled as follows: LP - long-pass filter, O - 20x objective, D - dichroic, BP -
621 bandpass filter, ND - neutral density filter, L - collimating lens, LED - light emitting diode, M1, M2
622 - fully reflective mirrors, CCD - Charge-Coupled Device Camera. LED power output is controlled
623 by the current from the LED driver, which is controlled by modulating the voltage through a
624 LabView interface. (B) Area captured by the camera compared to the total illumination area,
625 which is equal to the objective's field of view. Minimal and maximal distances that unexposed
626 bacteria need to swim to reach the observation area are shown.

22

627     **Figure 1 – figure supplement 2.** Estimating evenness of the Illumination profile from the

628     brightness of the image captured by the camera. (A) Blue light illumination profile captured by

629     the CCD camera. Color indicates normalized brightness of each pixel (brightness divided by the

630     average brightness). (B) Distribution of the normalized pixel brightness. The standard deviation

631     of the distribution is ~ 0.1.

632     **Figure 1 – figure supplement 3. Filtering spurious trajectories.** (A) Representative

633     two-dimensional distribution of ~200,000 trajectories from wild-type *E. coli* plotted against the

634     95th percentile of velocity and mean angular velocity. Trajectories outside the green contour with

635     radius $R = 4 <MAD>$ are removed from further analysis (Materials and Methods). Dots indicate

636     randomly selected trajectories shown in panel (B). (B) Each panel contains 100 randomly

637     selected trajectories from within each contour in panel (A). The color of the panel frame

638     indicates which region the trajectories come from in panel (A). (C) Fraction of trajectories within

639     each contour as indicated by the color, before, during, and after light exposure.

640     **Figure 1 – figure supplement 4. Blue light response under alternate growth conditions.**

641     Tumble bias trace for the wild-type strain RP437 grown in M9 minimal medium with glycerol and

642     resuspended in motility buffer with lactate (Materials and Methods). ~3000 trajectories were

643     used to calculated average tumble bias at each time point. Response to a turn-on of blue light of

644     intensity $44 \pm 4$ mW/cm$^2$ reproduces previous results on *E. coli* grown with the same carbon

645     source [7].

646     **Figure 1 – figure supplement 5. Response to light in *E. coli* is mediated by the**

647     **chemotaxis network.** Tumble bias traces for *E. coli* mutants lacking different components of

648     the chemotaxis network (Table 1): receptorless strain with all receptor types deleted (grey) [26],

649     ΔCheY strain lacking functional CheY (yellow) [52], ΔCheR strain lacking methylesterase CheR

650     (red), ΔCheB strain lacking methyltransferase CheB (green). ~500 - 3000 trajectories were used

651     to calculated average tumble bias at each time point. The wild-type response trace is shown for

23

652    comparison (blue). All responses were measured at a blue light intensity of $551 \pm 55$ mW/cm$^2$ as

653    indicated by the light intensity profile.

654    **Figure 2. Blue light response for single-receptor *E. coli* strains.** (A) Tumble bias traces for

655    single-receptor *E. coli* strains (Table 1): Aer-only (blue), Tar-only (green), Tsr-only (orange),

656    Trg-only (purple) and Tap-only (magenta). ~200 - 2000 trajectories were used to calculated

657    average tumble bias at each time point. Schematics indicate which receptor is present (filled

658    rectangles) and absent (empty rectangles) in each strain. All responses were measured at a

659    blue light intensity of $551 \pm 55$ mW/cm$^2$ as indicated by the light intensity profile. Grey dashed

660    lines show the prestimulus tumble bias for turn-on and turn-off responses. (B) Blue light-intensity

661    dependence of parameters for the responses to turn-on (filled circles) and turn-off (empty

662    circles) for all strains. Response amplitude, response time, and adaptation time were calculated

663    as illustrated by the schematics.

664    **Figure 2 – figure supplement 1. Effect of phenol on the light response in Tap-only and**

665    **Tar-only strain.** Tumble bias traces for Tap-only (magenta) and Tar-only (green) strains without

666    phenol (solid line), with 2.5 mM phenol (dashed line), and with 5 mM phenol (dotted line). ~200 -

667    2000 trajectories were used to calculated average tumble bias at each time point.

668    **Figure 2 – figure supplement 2. Blue light responses at different intensity levels for**

669    **Aer-only, Tar-only, and Trg-only strains.** Light intensity is indicated by the trace color. Grey

670    dashed lines show prestimulus tumble bias for turn-on and turn-off responses. Light exposure is

671    indicated by the shaded area as well as by the light intensity profile above the plot. ~200 - 2000

672    trajectories were used to calculated average tumble bias at each time point.

673    **Figure 3. Non-additivity of individual receptor responses in blue light response from**

674    **multiple-receptor strains.** (A) Tumble bias traces for $\Delta$Tsr$\Delta$Trg (red), $\Delta$Trg (dark blue) and $\Delta$Aer

675    (cyan) strains. Schematics indicate which receptor is present in each strain. All responses were

676    measured at a blue light intensity of $551 \pm 55$ mW/cm$^2$ as indicated by the light intensity profile.

24

677 ~900 - 4000 trajectories were used to calculated average tumble bias at each time point. (B)

678 Schematics of responses from single receptors that contribute to the observed responses from

679 multiple-receptor strains. The signs and kinetics of the multiple-receptor responses are different

680 from those expected from simple addition and is, therefore, a combined result of individual

681 receptor responses and their interactions. (C) Pie chart of the relative abundances of different

682 receptor types in the wild-type strain, based on data from [21].

683 **Figure 4. Effect of light on running velocity.** (A) Light exposure causes a reversible decrease

684 in swimming velocity. Normalized velocity traces are shown for receptorless strain UU1250.

685 ~2000 trajectories were used to calculated velocity at each time point. Light intensity is indicated

686 by the trace color. The velocity is normalized by its prestimulus value (calculated in a 20 s

687 window before light exposure; Materials and Methods). (B) Bar plot of the normalized swimming

688 velocity for different *E. coli* strains. The normalized velocity was calculated in a 4-s window after

689 30 s of exposure to light, then 10, 20, and 30 s after the light was turned off. Light exposure and

690 intensity are indicated by the intensity profile above the plot. (C) Dependence of velocity

691 decrease and recovery on light intensity. Velocity decrease, $\Delta v_{on}$, and velocity recovery, 1 -

692 $\Delta v_{on}/\Delta v_{off}$, were calculated as illustrated by the schematic in (B). Velocity recovery is shown 10,

693 20, and 30 s after light turn-off as indicated by the color.

694

# References

695

1. Häder DP. Photosensory behavior in procaryotes. Microbiol Rev. 1987;51: 1–21.

2. Armitage JP, Hellingwerf KJ. Light-induced behavioral responses ('phototaxis') in prokaryotes. Photosynth Res. 2003;76: 145–155. doi:10.1023/A:1024974111818

3. Purcell EB, Crosson S. Photoregulation in prokaryotes. Curr Opin Microbiol. 2008;11: 168–178. doi:10.1016/j.mib.2008.02.014

4. Taylor BL, Koshland DE. Intrinsic and extrinsic light responses of Salmonella typhimurium and Escherichia coli. J Bacteriol. 1975;123: 557–569.

5. Taylor BL, Miller JB, Warrick HM, Koshland DE. Electron acceptor taxis and blue light effect on bacterial chemotaxis. J Bacteriol. 1979;140: 567–573.

6. Yang H, Inokuchi H, Adler J. Phototaxis away from blue light by an Escherichia coli mutant accumulating protoporphyrin IX. Proc Natl Acad Sci U S A. 1995;92: 7332–7336.

7. Wright S, Walia B, Parkinson JS, Khan S. Differential activation of Escherichia coli chemoreceptors by blue-light stimuli. J Bacteriol. 2006;188: 3962–3971. doi:10.1128/JB.00149-06

8. Mears PJ, Koirala S, Rao CV, Golding I, Chemla YR. Escherichia coli swimming is robust against variations in flagellar number. Elife. 2014; 1–18. doi:10.7554/eLife.01916

9. Rebbapragada A, Johnson MS, Harding GP, Zuccarelli AJ, Fletcher HM, Zhulin IB, Taylor BL. The Aer protein and the serine chemoreceptor Tsr independently sense intracellular energy levels and transduce oxygen, redox, and energy signals for Escherichia coli behavior. Proceedings of the National Academy of Sciences. 1997;94: 10541–10546. doi:10.1073/pnas.94.20.10541

10. Sourjik V, Wingreen NS. Responding to chemical gradients: bacterial chemotaxis. Curr Opin Cell Biol. Elsevier Ltd; 2012;24: 262–268. doi:10.1016/j.ceb.2011.11.008

11. Grebe TW, Stock J. Bacterial chemotaxis: the five sensors of a bacterium. Curr Biol. 1998;8: R154–7.

12. Yang Y, Sourjik V. Opposite responses by different chemoreceptors set a tunable preference point in Escherichia coli pH taxis. Mol Microbiol. 2012;86: 1482–1489. doi:10.1111/mmi.12070

13. Sourjik V, Wingreen NS. Responding to chemical gradients: bacterial chemotaxis. Curr Opin

724       Cell Biol. Elsevier Ltd; 2012;24: 262–268. doi:10.1016/j.ceb.2011.11.008

725  14. Mao H, Cremer PS, Manson MD. A sensitive, versatile microfluidic assay for bacterial
726       chemotaxis. Proc Natl Acad Sci U S A. 2003;100: 5449–5454.
727       doi:10.1073/pnas.0931258100

728  15. Paster E, Ryu WS. The thermal impulse response of Escherichia coli. Proc Natl Acad Sci U
729       S A. 2008;105: 5373–5377. doi:10.1073/pnas.0709903105

730  16. Taylor BL, Zhulin IB, Johnson MS. Aerotaxis and other energy-sensing behavior in bacteria.
731       Annu Rev Microbiol. 1999;53: 103–128. doi:10.1146/annurev.micro.53.1.103

732  17. Baker MD, Wolanin PM, Stock JB. Signal transduction in bacterial chemotaxis. Bioessays.
733       2006;28: 9–22. doi:10.1002/bies.20343

734  18. Berg HC. Motile Behavior of Bacteria. Phys Today. 2000;53: 24. doi:10.1063/1.882934

735  19. Hazelbauer GL, Falke JJ, Parkinson JS. Bacterial chemoreceptors: high-performance
736       signaling in networked arrays. Trends Biochem Sci. 2008;33: 9–19.
737       doi:10.1016/j.tibs.2007.09.014

738  20. Vladimirov N, Sourjik V. Chemotaxis: how bacteria use memory. Biol Chem. Walter de
739       Gruyter und Co., Genthiner Str. 13 Berlin 10785 Germany; 2009;390: 1097–1104.
740       doi:10.1515/BC.2009.130

741  21. Li M, Hazelbauer GL. Cellular Stoichiometry of the Components of the Chemotaxis
742       Signaling Complex. 2004;186: 3687–3694. doi:10.1128/JB.186.12.3687

743  22. Barnakov AN, Barnakova LA, Hazelbauer GL. Comparison in vitro of a high- and a
744       low-abundance chemoreceptor of Escherichia coli: Similar kinase activation but different
745       methyl-accepting activities. J Bacteriol. 1998;180: 6713–6718.

746  23. Yamamoto K, Macnab RM, Imae Y. Repellent response functions of the Trg and Tap
747       chemoreceptors of Escherichia coli. J Bacteriol. 1990;172: 383–388.

748  24. Berman - Academic Press IB, York N, 1971. Handbook of fluorescence spectra of aromatic
749       molecules. 1971;

750  25. Yuan J, Branch RW, Hosu BG, Berg HC. Adaptation at the output of the chemotaxis
751       signalling pathway. Nature. Nature Publishing Group; 2012;484: 233–236.
752       doi:10.1038/nature10964

753  26. Bibikov SI, Miller AC, Gosink K, Parkinson JS. Methylation-independent aerotaxis mediated
754       by the Escherichia coli Aer protein. J Bacteriol. 2004;186: 3730–3737.

27

755      doi:10.1128/JB.186.12.3730

756   27. Vladimirov N, Løvdok L, Lebiedz D, Sourjik V. Dependence of bacterial chemotaxis on
757      gradient shape and adaptation rate. PLoS Comput Biol. 2008;4: e1000242.
758      doi:10.1371/journal.pcbi.1000242

759   28. Min TL, Mears PJ, Golding I, Chemla YR. Chemotactic adaptation kinetics of individual
760      Escherichia coli cells. Proceedings of the National Academy of Sciences. 2012;109: 1–6.
761      doi:10.1073/pnas.1120218109

762   29. Parkinson JS. Crosslinking snapshots of bacterial chemoreceptor squads. 2004;101:
763      6314–6318. doi:10.1073/pnas.1115170108

764   30. Briegel A, Li X, Bilwes AM, Hughes KT, Jensen GJ, Crane BR. Bacterial chemoreceptor
765      arrays are hexagonally packed trimers of receptor dimers networked by rings of kinase and
766      coupling proteins. Proceedings of the National Academy of Sciences. 2012;109:
767      3766–3771. doi:10.1073/pnas.1115719109

768   31. Parkinson JS, Hazelbauer GL, Falke JJ. Signaling and sensory adaptation in Escherichia
769      coli chemoreceptors: 2015 update. Trends Microbiol. Elsevier Ltd; 2015; 1–10.
770      doi:10.1016/j.tim.2015.03.003

771   32. Sourjik V, Berg HC. Receptor sensitivity in bacterial chemotaxis. Proc Natl Acad Sci U S A.
772      2002;99: 123–127. doi:10.1073/pnas.011589998

773   33. Lan G, Schulmeister S, Sourjik V, Tu Y. Adapt locally and act globally: strategy to maintain
774      high chemoreceptor sensitivity in complex environments. Mol Syst Biol. Nature Publishing
775      Group; 2011;7: 475. doi:10.1038/msb.2011.8

776   34. Taylor BL. Aer on the inside looking out: paradigm for a PAS-HAMP role in sensing oxygen,
777      redox and energy. Mol Microbiol. 2007;65: 1415–1424.
778      doi:10.1111/j.1365-2958.2007.05889.x.Aer

779   35. White David. Membrane Bioenergetics: The Proton Potential. PLoS Comput Biol. Oxford
780      University Press; 2012;10: e1003870. doi:10.1371/journal.pcbi.1003870

781   36. Fung DC, Berg HC. Powering the flagellar motor of Escherichia coli with an external voltage
782      source [Internet]. Nature. 1995. pp. 809–812. doi:10.1038/375809a0

783   37. Gabel CV, Berg HC. The speed of the flagellar rotary motor of Escherichia coli varies
784      linearly with protonmotive force. Proc Natl Acad Sci U S A. 2003;100: 8748–8751.
785      doi:10.1073/pnas.1533395100

786   38. Nakamura S, Nakamura T, Ogura Y. Absorption spectrum of flavin mononucleotide

787      semiquinone. J Biochem. 1963;53: 143–146.

788  39. Losi A, Gärtner W. Old chromophores, new photoactivation paradigms, trendy applications:
789      flavins in blue light-sensing photoreceptors. Photochem Photobiol. 2011;87: 491–510.
790      doi:10.1111/j.1751-1097.2011.00913.x

791  40. Conrad KS, Manahan CC, Crane BR. Photochemistry of flavoprotein light sensors. Nat
792      Chem Biol. Nature Publishing Group; 2014;10: 801–809. doi:10.1038/nchembio.1633

793  41. Kao Y-T, Saxena C, He T-F, Guo L, Wang L, Sancar A, Zhong D. Ultrafast dynamics of
794      flavins in five redox states. J Am Chem Soc. 2008;130: 13132–13139.
795      doi:10.1021/ja8045469

796  42. Edwards JC, Johnson MS, Taylor BL. Differentiation between electron transport sensing
797      and proton motive force sensing by the Aer and Tsr receptors for aerotaxis. Mol Microbiol.
798      2006;62: 823–837. doi:10.1111/j.1365-2958.2006.05411.x

799  43. Blount ZD. The unexhausted potential of E. coli. Elife. 2015;4. doi:10.7554/eLife.05826

800  44. Kalinin Y, Neumann S, Sourjik V, Wu M. Responses of Escherichia coli bacteria to two
801      opposing chemoattractant gradients depend on the chemoreceptor ratio. J Bacteriol.
802      2010;192: 1796–1800. doi:10.1128/JB.01507-09

803  45. Bradski G. Open Source Computer Vision Library. Dr Dobb's Journal of Software Tools.
804      2000;

805  46. Allan D, Caswell TA, Keim N, Boulogne F, Perry RW, Uieda L. trackpy: Trackpy v0.3.0.
806      2014. doi:10.5281/zenodo.12255

807  47. Dufour YS, Gillet S, Frankel NW, Weibel DB, Emonet T. Direct Correlation between Motile
808      Behavior and Protein Abundance in Single Cells. Stock AM, editor. PLoS Comput Biol.
809      2016;12: e1005041. doi:10.1371/journal.pcbi.1005041

810  48. Pedregosa F, Varoquaux G, Gramfort A, Michel V, Thirion B, Grisel O, Blondel M,
811      Prettenhofer P, Weiss R, Dubourg V, Vanderplas J, Passos A, Cournapeau D, Brucher M,
812      Perrot M, Duchesnay E. Scikit-learn: Machine Learning in Python. J Mach Learn Res.
813      2011;12: 2825–2830.

814  49. Alon U, Camarena L, Surette MG, Aguera y Arcas B, Liu Y, Leibler S, Stoc J B. Response
815      regulator output in bacterial chemotaxis. EMBO J. 1998;17: 4238–4248.
816      doi:10.1093/emboj/17.15.4238

817  50. Khan S, Castellano F, Spudich JL, McCray JA, Goody RS, Reid GP, Trentham D R.
818      Excitatory signaling in bacterial probed by caged chemoeffectors. Biophys J. 1993;65:

29

819        2368–2382. doi:10.1016/S0006-3495(93)81317-1

820    51. Parkinson JS, Houts SE. Isolation and Behavior of Escherichia coli Deletion Mutants
821        Lacking Chemotaxis Functions. 1982;

822    52. Min TL, Mears PJ, Chubiz LM, Rao CV, Golding I, Chemla YR. High-resolution, long-term
823        characterization of bacterial motility using optical tweezers. Nat Methods. Nature Publishing
824        Group; 2009;6: 831–835. doi:10.1038/nmeth.1380

825    53. Gosink KK, Burón-Barral M del C, Parkinson JS. Signaling interactions between the
826        aerotaxis transducer Aer and heterologous chemoreceptors in Escherichia coli. J Bacteriol.
827        2006;188: 3487–3493. doi:10.1128/JB.188.10.3487-3493.2006

828    54. Bibikov SI, Biran R, Rudd KE, Parkinson JS. A signal transducer for aerotaxis in
829        Escherichia coli. J Bacteriol. 1997;179: 4075–4079.

# Figure 1
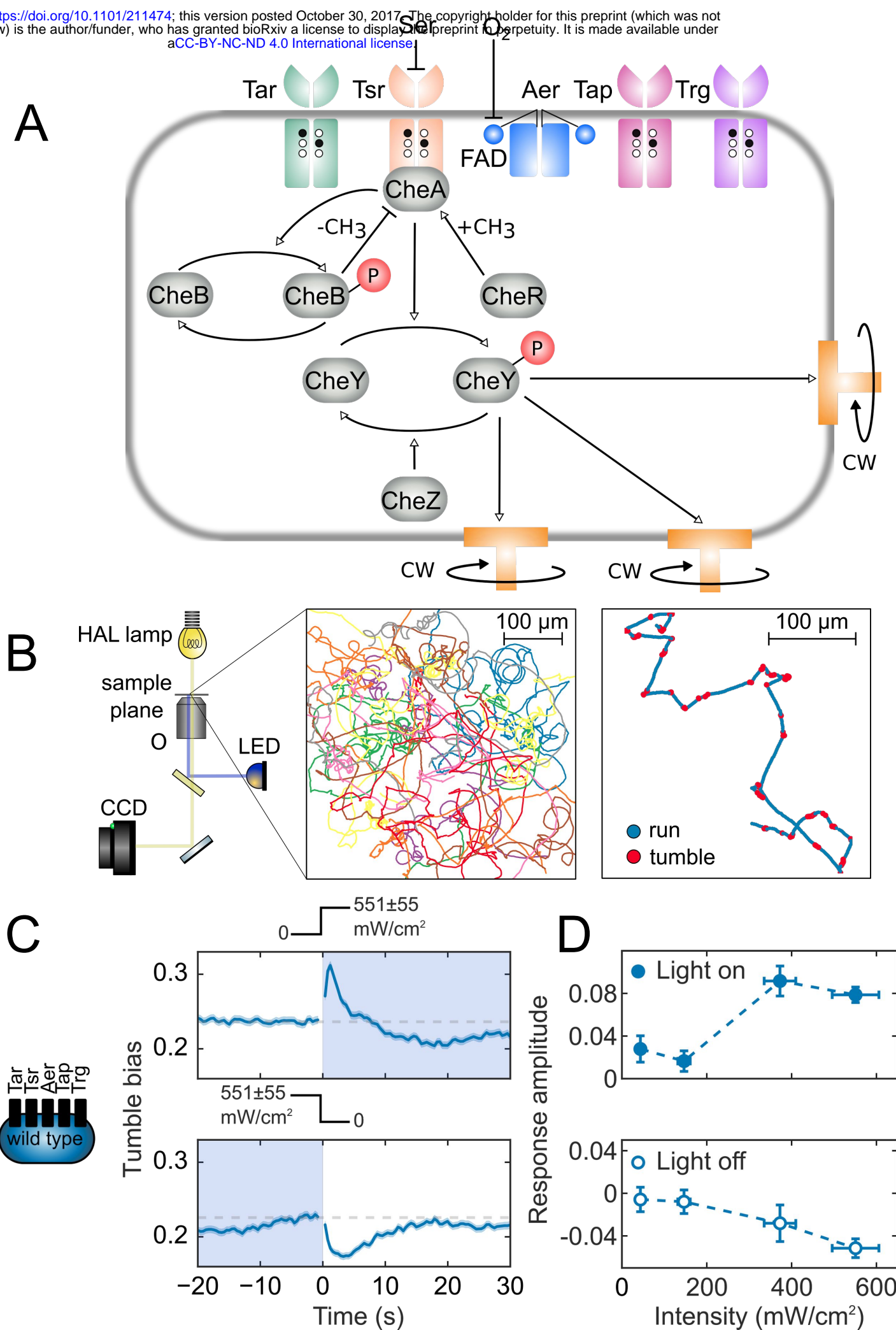
# Figure 1 - Supplement figure 1
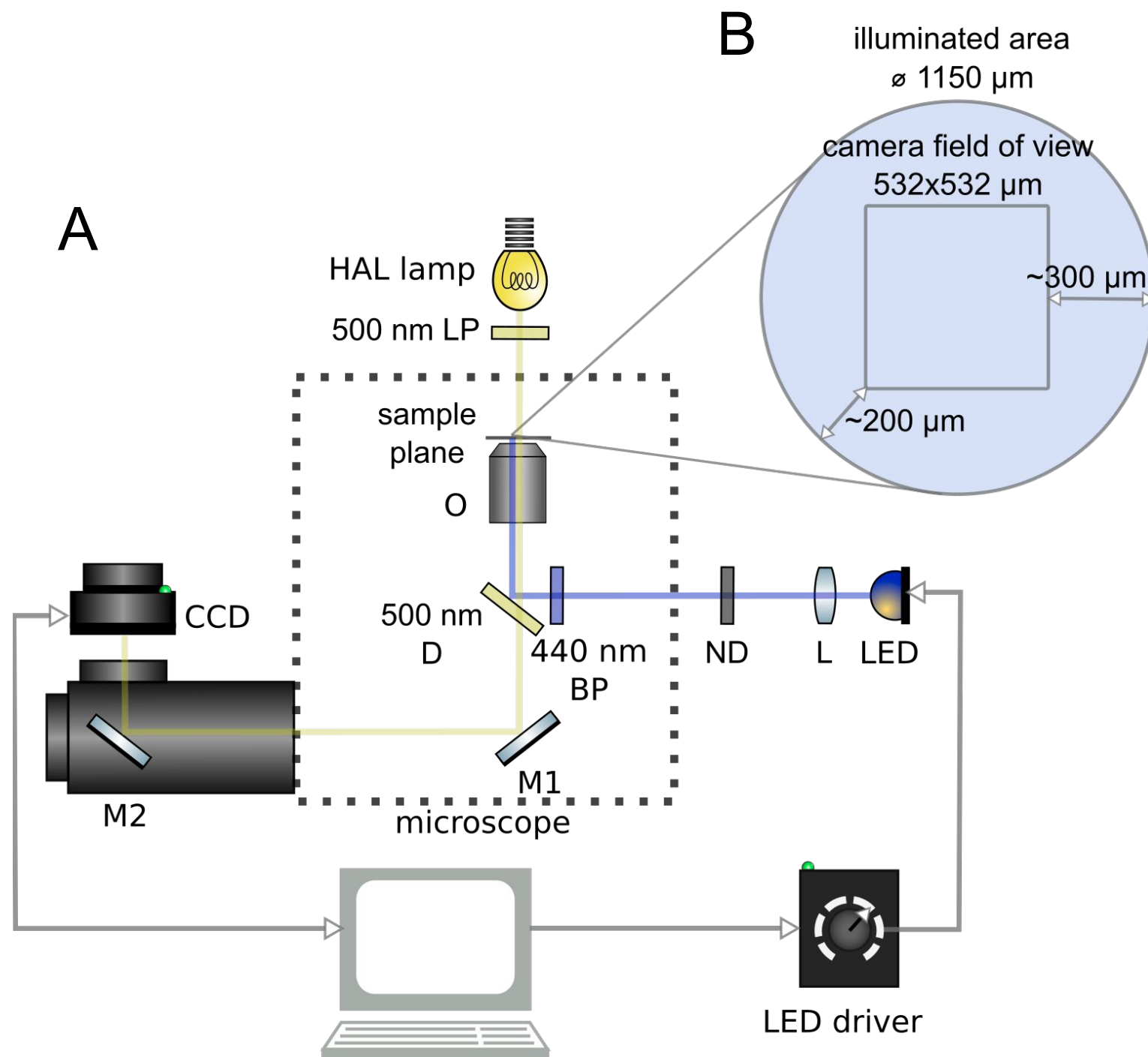
# Figure 1 - Supplement figure 2
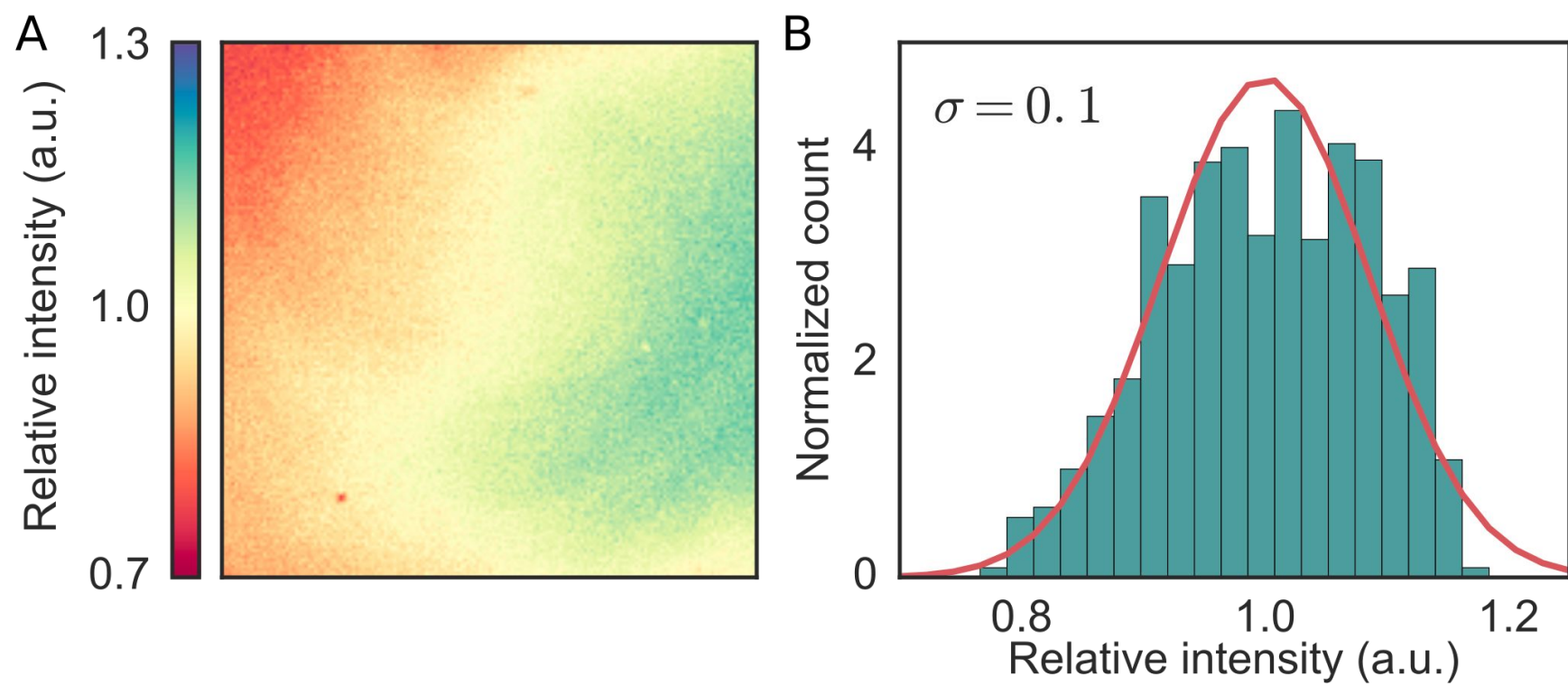
# Figure 1 - Supplement figure 3
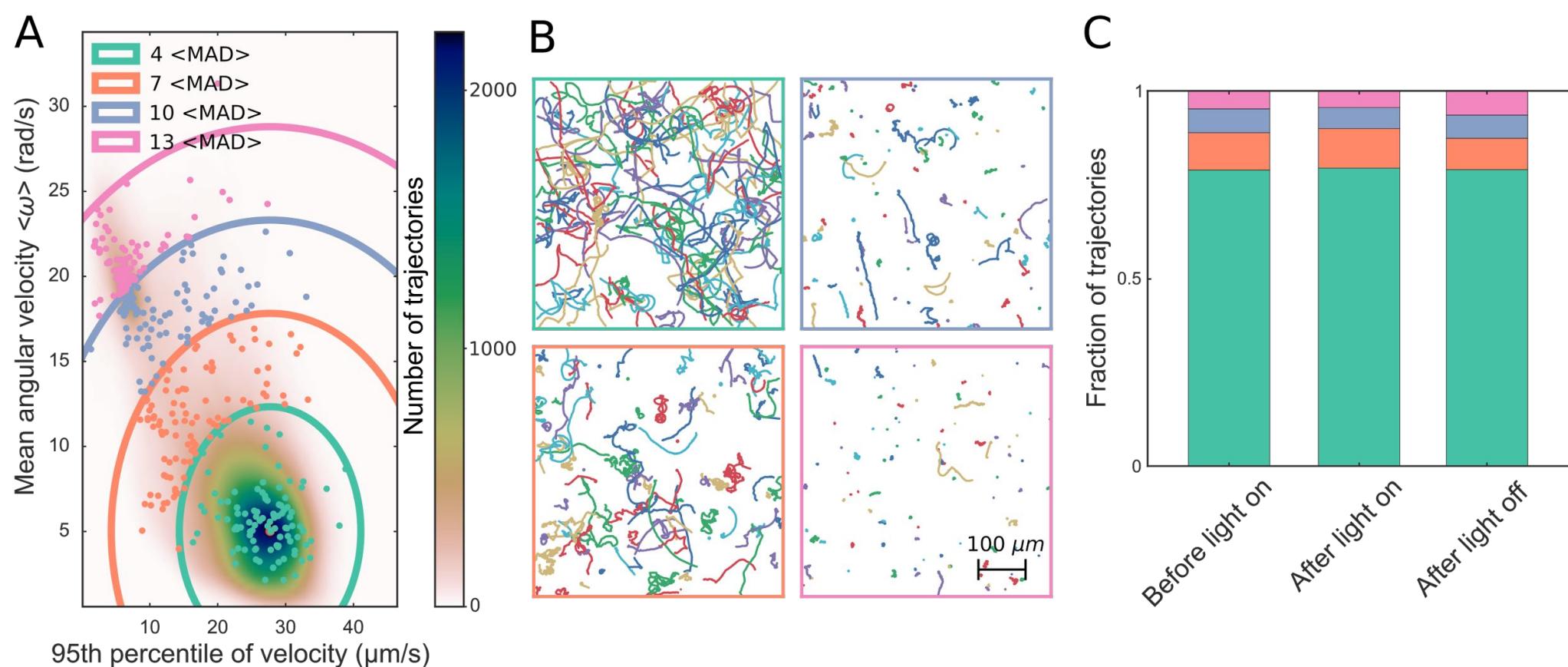
# Figure 1 - Supplement figure 4
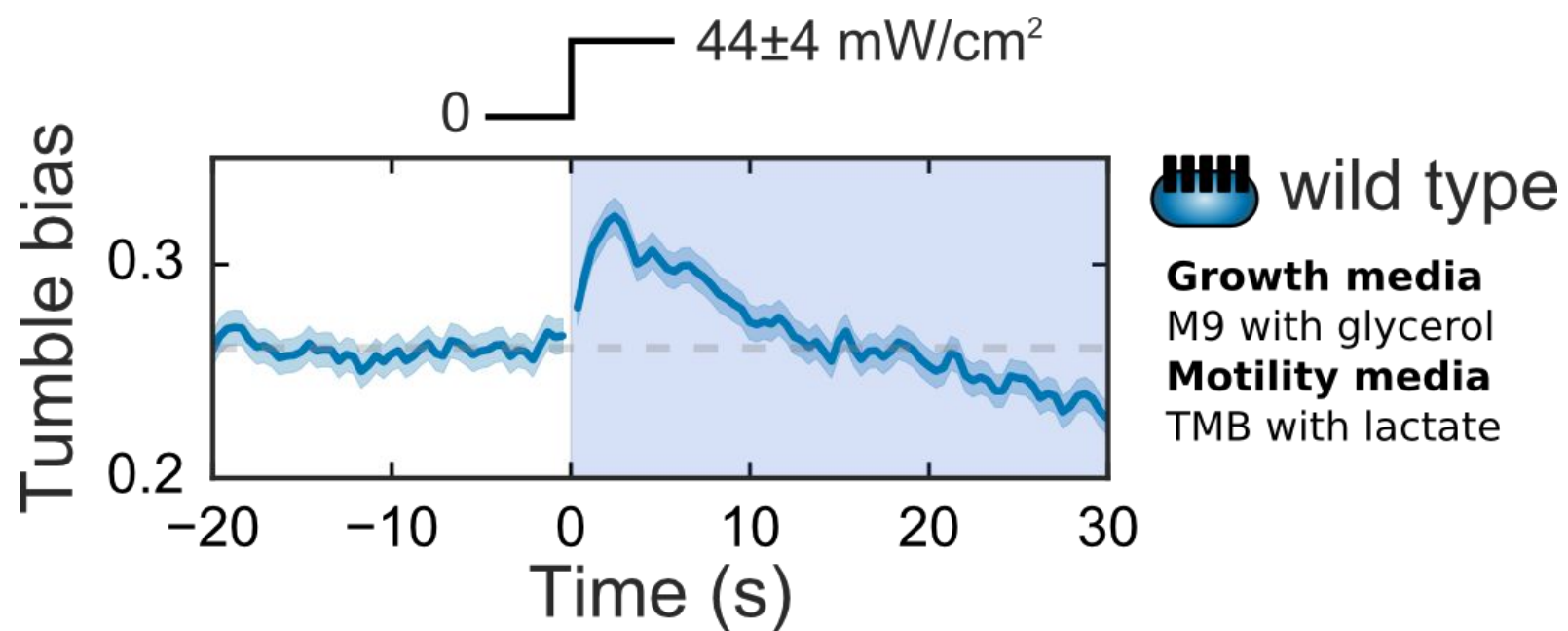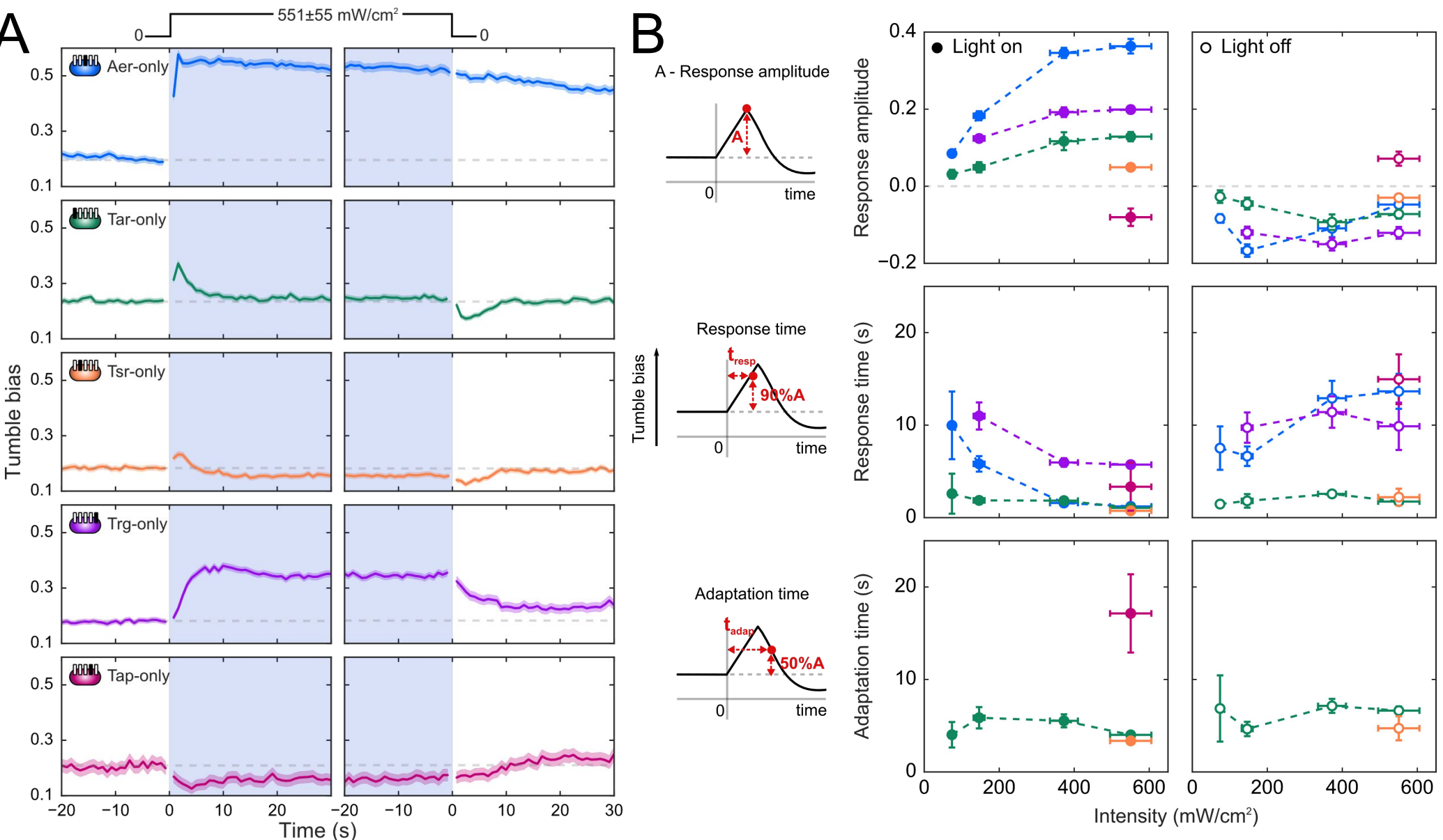
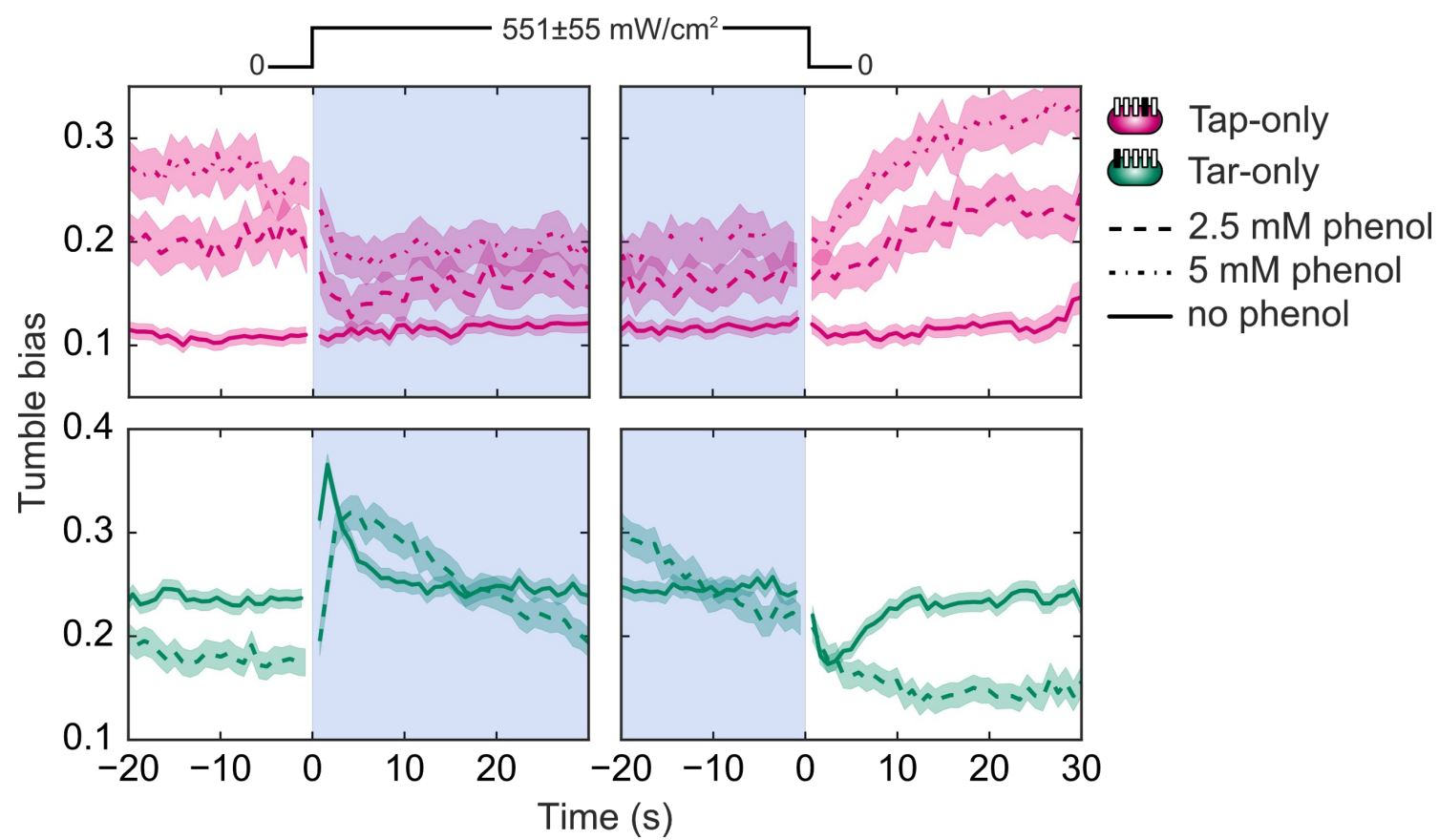# Figure 1 - Supplement figure 5
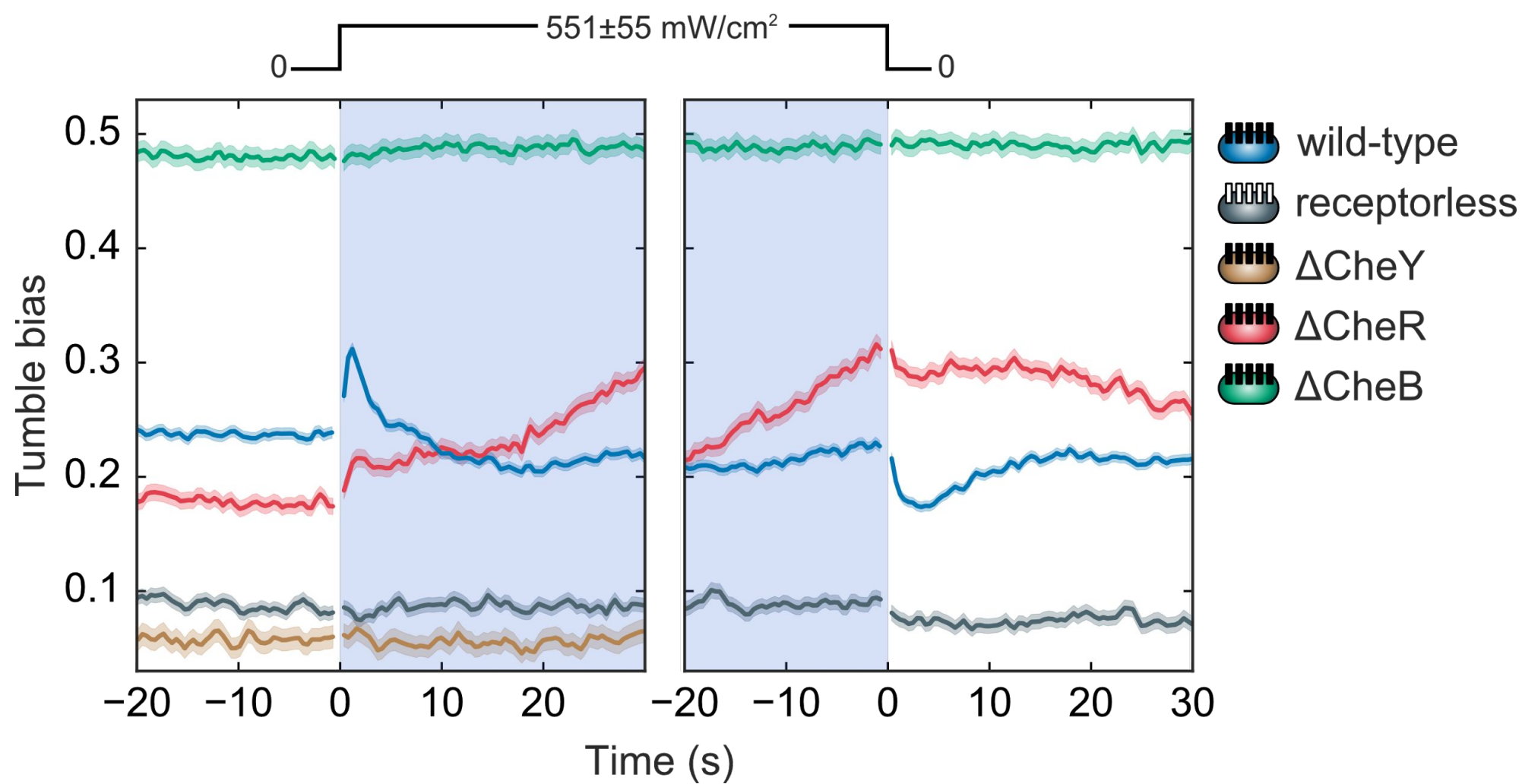
# Figure 2

# Figure 2 - Supplement figure 1
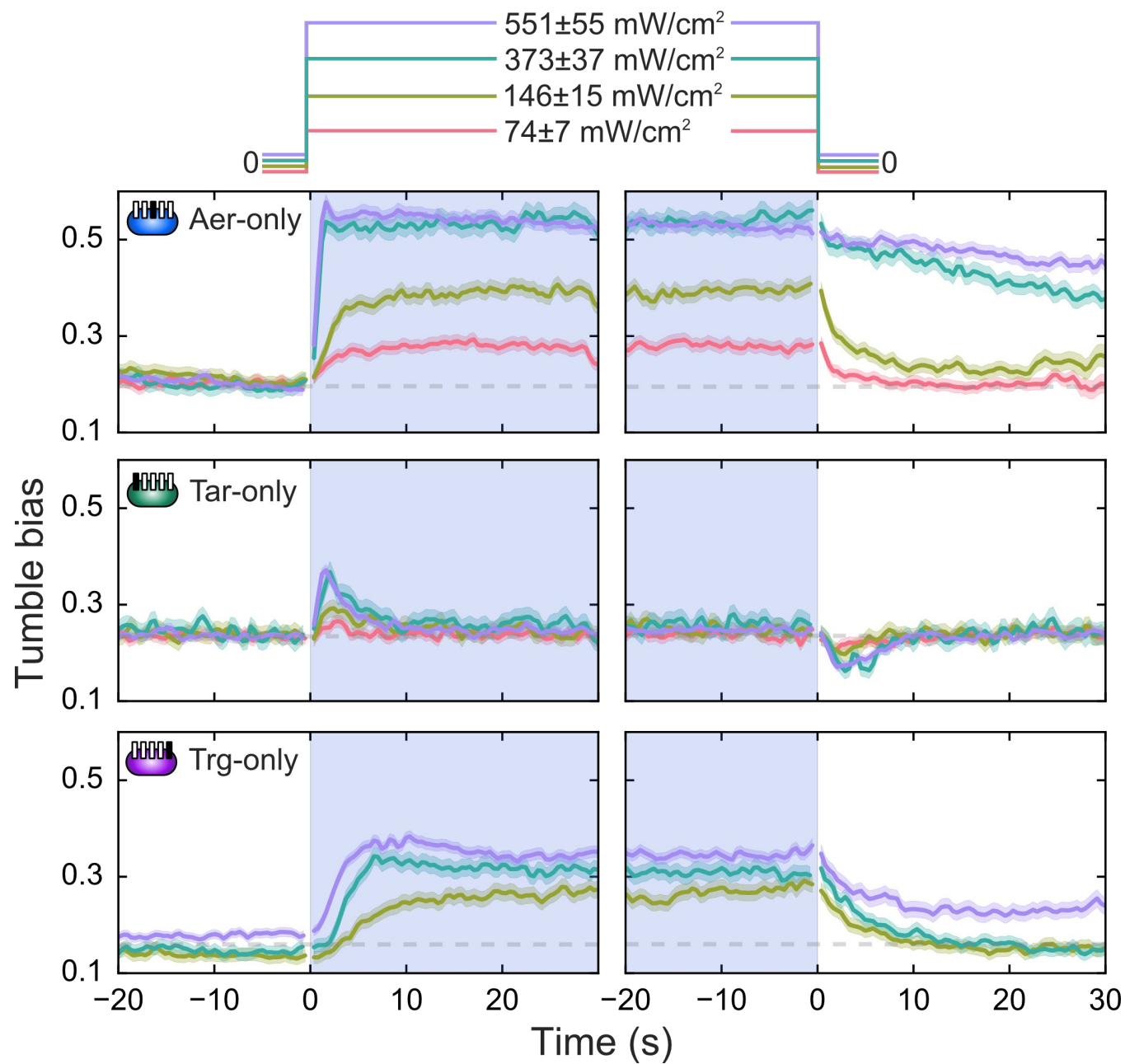
# Figure 2 - Supplement figure 2

# Figure 3

# Figure 4